



Full length article

Design of efficient bi-orthogonal wavelets for EEG-based detection of Schizophrenia

Digambar V. Puri ^a, Pramod H. Kachare ^a, Ibrahim Al-Shourbaji ^b, Abdoh Jabbari ^b,
Raimund Kirner ^c, Abdalla Alameen ^d

^a Department of Computer Science Engineering, RAIT, D Y Patil Deemed to be University, Navi-Mumbai, 400706, India

^b Department of Electrical and Electronics Engineering, Jazan University, Jazan, Saudi Arabia

^c Department of Computer Science, University of Hertfordshire, Hatfield AL10 9AB, UK

^d Department of Computer Engineering and Information, Prince Sattam Bin Abdulaziz University, Wadi Alddawasir 11991, Saudi Arabia

ARTICLE INFO

Keywords:

Electroencephalogram
Schizophrenia
Filter banks
Wavelets
LS-SVM

ABSTRACT

The state-of-the-art bi-orthogonal wavelet filters need infinite precision implementation due to more number of irrational filter coefficients. This paper presents a novel low-complexity bi-orthogonal wavelet filter-bank (LCBWFB) with canonical-signed-digit filters to reduce the computations. The proposed wavelet filter design uses a generalized matrix formulation technique with sharp roll-off to generate rational coefficients. These filters facilitate near-orthogonality, regularity, and perfect reconstruction. Different lengths of highpass and lowpass filters are generated by varying the half-band polynomial factors. The various combinations of filter banks including 9/7, 10/6, and 11/9 are designed using proposed method. This method provides the freedom to select the parameters according to the size of the filter bank. Comparative analysis with earlier reported bi-orthogonal wavelets showed lower computations and higher regularity for the LCBWFB. These rational coefficients are then used in automatic schizophrenia detection to decompose EEG signals. The Fisher score is used to select the most discriminating channels, and each channel is decomposed using LCBWFB into six subbands. A set of 22 features, comprising statistical, entropy, and complexity, are calculated for each subband. A least square support vector machine is tuned using the Grey Wolf optimizer and is trained using the five most significant features selected using the Wilcoxon Signed-rank test. The 10-fold accuracy of 96.84%, sensitivity of 95.95%, and specificity of 96.97%. These values using leave-one-subject-out are 93.92%, 92.30%, and 93.77%, respectively, obtained for an open-source dataset with only 25 out of 1408 features comparable to existing Schizophrenia detection methods.

1. Introduction

Schizophrenia (SCZ) is a neuro-psychiatric chronic disorder that directly affects the emotional behavior, thinking, hallucinations, and delusions [1]. According to World Health Organization (WHO) figures, approximately 25 million people have suffered from SCZ disease in 2023 [2]. People in their early twenties are more likely to develop SCZ disease. The main characteristic symptoms are cognitive dysfunctions and negative and positive symptoms [3]. The primary reasons for increasing SCZ mortality are delays in the treatment and misdiagnosis of SCZ patients. The WHO stated long-term, expensive medication in the treatment of SCZ that can cause a massive burden on families and healthcare systems. The early diagnosis can prevent the severe stage of SCZ and can be delayed by medication [4]. Hence, an automatic, cost-effective, and reliable SCZ detection system is required.

Recently, different modalities are available for the detection of SCZ like functional magnetic resonance imaging (fMRI), resting state MRI [5], mini-mental state examination, and Electroencephalogram (EEG). Out of these EEG has shown promising results in the detection of neurological disorders such as, epilepsy [6], alcoholism [7], evoked emotions [8], Alzheimer's disease [9] and changes in brain functions. Moreover, it provides a high temporal resolution that has attracted researchers and neuro-experts [10].

Several EEG-based methods for diagnosis of SCZ are summarized in Table 1, which includes dataset details, methods used for feature extraction, and classification with their performances. In the literature [27,30,31], the time domain non-linear features were extracted to diagnose the SCZ from normal healthy controlled subjects (NHC). Moreover, frequency domain features like statistical parameters

* Corresponding author.

E-mail addresses: digambar.puri@rait.ac.in (D.V. Puri), r.kirner@herts.ac.uk (R. Kirner).

<https://doi.org/10.1016/j.jestch.2025.102090>

Received 24 January 2025; Received in revised form 4 May 2025; Accepted 12 May 2025

Available online 4 June 2025

2215-0986/© 2025 The Authors. Published by Elsevier B.V. on behalf of Karabuk University. This is an open access article under the CC BY license (<http://creativecommons.org/licenses/by/4.0/>).

Table 1
Related state-of-art methods for diagnosis of Schizophrenia.

Author	Year	Dataset	C*	Method	CV	Classifier	ACCY	SENS	SPEC
Ali et al. [11]	2025	IPN, Poland 14 SCZ, 14 NHC	19	TQWT and STFT based features	–	DA-Bi-LSTM	93.13	91.30	95.04
Senathi et al. [12]	2025	Chennai, India 36 SCZ, 22 NHC	19	ResDense deep features	–	Transformer model	96.00	97.00	98.24
Yin et al. [13]	2025	Beijing Huilongguan Hospital 103 SCZ, 92 NHC	59	Spatial, frequency features	–	3D-AGCNN	87.64	92.73	85.77
Shen et al. [14]	2024	Mental health research center, Moscow state university 45 SCZ, 39 NHC	16	MVAR coherence features	10-fold	3D-CNN	98.47	99.26	97.23
Hussain et al. [15]	2024	Mental health research center, Moscow state university 45 SCZ, 39 NHC	16	Deep features	10-fold	Lightweight CNN	92.38	94.44	90.00
Aziz et al. [16]	2024	Mental health research center, Moscow state university 45 SCZ, 39 NHC	16	Deep features	10-fold	Lightweight CNN	96.70	96.80	97.00
Kumar et al. [17]	2023	Mental health research center, Moscow state university 45 SCZ, 39 NHC	16	Correlation-based feature selection	10 fold	Adaboost	92.85	93.30	92.30
Sahu et al. [18]	2023	IPN, Poland 14 SCZ, 14 NHC	19	Multi-DWT	16	AdaBoost	85.71	90.00	81.81
Miras et al. [19]	2023	Hospital Universitario San Agustin, Jaen	19	Non-linear features	10 fold	KNN	87.00	82.00	90.00
Aksoz et al. [20]	2022	IPN, Poland 14 SCZ, 14 NHC	19	Hjorth parameter features	10 fold	ANN	93.90	–	–
Keihani et al. [21]	2022	IPN, Poland 14 SCZ, 14 NHC	19	Global Field Power Bayesian Optimization	10-fold	SVM	90.93	91.37	90.48
Zandbagleh et al. [22]	2022	Nottingham Trent University 25 SCZ, 25 NHC	64	MVAR-based connectivity measure	LOSO	SVM	89.21	90.30	88.20
Khare et al. [23]	2021	University of California at San Francisco 49 SCZ, 32 NHC	64	FTQWT	10 fold	FLS- LSSVM	91.39	92.65	93.22
Khare et al. [24]	2021	University of California at San Francisco 49 SCZ, 32 NHC	64	OVMD	10 fold	OELM	92.93	97.15	91.06
Kandala et al. [25]	2021	Neuro-physiology and neuro-computer interface, MHRC	16	Weighted local binary pattern and correlation	10-fold	Logit boost	91.66	–	–
Khare et al. [26]	2021	University of California at San Francisco 49 SCZ, 32 NHC	64	SPWVD	10 fold	CNN	93.36	94.25	92.03
Prabhakar et al. [27]	2020	IPN, Polandr 14 SCZ, 14 NHC	19	Nonlinear features	10 fold	SVM	89.85	–	–
Khare et al. [1]	2020	University of California at San Francisco 49 SCZ, 32 NHC	64	EWT-based features	10 fold	SVM	89.59	89.76	89.32
Phang et al. [28]	2020	Mental health research center, Moscow state university 45 SCZ, 39 NHC	16	Time-frequency domain VAR	5 fold	CNN	91.69	91.11	92.50
Naira et al. [29]	2020	Mental health research center, Moscow state university 45 SCZ, 39 NHC	16	Pearson correlation coefficient	–	CNN	90.00	90.00	90.00

MEMD: Multivariate empirical mode decomposition, STFT: short-time Fourier transform, CWT-continuous wavelet transform, TQWT: Tunable Q-wavelet transform, F-TQWT: Flexible TQWT, OVMD: optimized variational mode decomposition, HFD: Higuchi's fractal dimension, FFT: fast Fourier transform, CNN: Convolutional neural network, DT: decision tree, SVM: support vector machine, KNN: k-nearest neighbor, RF: random forest, LSSVM: least square SVM, KFD: Karl's fractal dimension, ANN: Artificial neural network, DWT: Discrete wavelet transform, LDA: Linear discriminant analysis, LZC: Lampel-Ziv complexity, SPWVD: Smoothed Pseudo Wigner-Ville distribution, VAR: Vector auto-regressive. C*: number of EEG Channels.

and complexity-based features have been reported to diagnose SCZ [20,32–35]. To improve the performance of the SCZ, the wavelet-based analysis has been carried out in various studies [18,23,36]. Recently, Krishnan et al. [37] investigated multivariate empirical mode decomposition (MEMD)-based on different entropy features. They reported a maximum 93% classification rate to diagnose the SCZ. Sharma et al. [38] proposed a computer-aided SCZ diagnosis system with only a single EEG channel. They computed the $l1$ -norm features from the seven subbands. The EEG signals were decomposed using a root mean square Butterworth filter. These features were fed to various machine

learning models and obtained the best accuracy of 98.21%. However, this performance is not consistent. Das et al. [39] introduced a method employing multivariate iterative filtering for detecting SCZ. The intrinsic mode functions (IMFs) are generated from different EEG rhythms based on their mean frequency. Thirty different features are extracted from each IMF. The classification was performed on K-nearest neighbors (KNN), linear discriminate analysis (LDA), and support vector machine (SVM). Among these, the SVM achieved the highest accuracy at 98.90%. Similarly, Gosala et al. [40] computed the statistical features from subbands obtained from wavelet scattering transform.

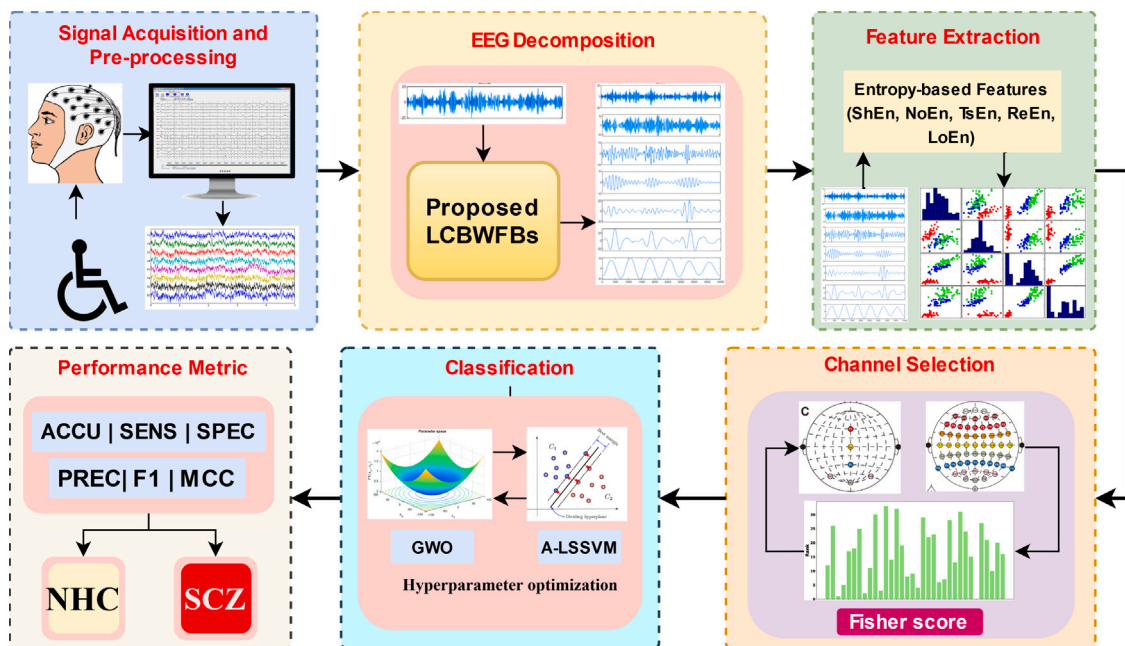


Fig. 1. Proposed LCBWFBs for automatic schizophrenia detection.

They reported the best classification accuracy of 97.98% with random forest (RF). From the above discussion it is clear that wavelets play significant role in the SCZ detection from the EEG signals. Ali et al. [11] reported a wavelet and Fourier based features with Bi-LSTM to detect SCZ. They obtained the 93.13% classification accuracy. However, the computation complexity is very high. The other deep learning-based approach using ResDense features and transformer model has been investigated by Senathi et al. [12]. Yin et al. used spatial and frequency-based features with the 3D-AGCNN model. However, this model did not provide promising results and managed to obtain 87.64% accuracy.

In the literature, a variety of wavelets are available. The most prevalent ones fall into the categories of orthogonal and bi-ortho. transform. A method to design compactly supported wavelets have introduced by Daubechies [41]. The orthogonal wavelets effectively rejects the amplification of noise in subbands using simplified coding design. However, these wavelets lack linearity and symmetry. This is crucial for managing distortions in finite length signals, such as EEG [42]. The linear phase and orthogonality have achieved only in Haar wavelet filters that are discontinuous [43]. The linearity can be achieved by relaxing the orthogonality of the wavelets or the use of bi-orthogonal wavelets. The popular bi-orthogonal wavelets are constructed using Cohen Daubechies Feauveau (CDF) 9/7 [43]. These wavelets provide the linear phase. However, these wavelets have irrational filter coefficients with higher lengths that increase the computational complexity of implementing them on hardware. Cheng et al. [44] utilized the lifting structure to obtain the binary wavelet filter coefficients by reducing the number of vanishing moments. The reduction in the vanishing moments results in a loss of frequency response control of the analysis and synthesis filter simultaneously. Patil et al. [45] designed bi-orthogonal wavelets using a general half-band filter polynomial. The flexibility in the wavelet coefficients has been obtained by reducing the VMs and adjusting the free parameters. However, for improving the flatness higher degree polynomial is essential, this results in higher filter length. These wavelets are not suitable for EEG signals due to low regularity and flatness.

Therefore, to overcome the above-mentioned issues, a new class of bi-orthogonal wavelet filter banks (LCBWFBs) have been designed using the proposed algorithm. The design uses a generalized matrix formulation technique with sharp roll-off to generate rational coefficients. These coefficients facilitate near-orthogonality, regularity, and

perfect reconstruction. Different length high and lowpass filters can be generated by varying the half-band polynomial factors. Comparative analysis with previously reported designs showed lower computations and high regularity for the LCBWFB. These rational coefficient filters are then used in automatic schizophrenia detection to decompose EEG signals. Here, we initiated the design of a half-band polynomial (HBP) to achieve a specific length. A method has been proposed for designing HBP with the maximum number of VMs. The synthesis and analysis filters are designed using a generalized matrix formulation technique with sharp roll-off. Consequently, various wavelets can be achieved with different properties and lengths. The performance of the proposed wavelets has been compared with existing bi-orthogonal wavelets. Further, these designed LCBWFBs are used to decompose the SCZ EEG signals for feature extraction. These extracted features were classified using adaptive least square SVM (ALSSVM). The hyper-parameters and kernel of ALSSVM are optimized using the well-known Grey Wolf optimization (GWO) [46] algorithm. The proposed automatic EEG-based SCZ detection (AESD) system is presented in Fig. 1. The performance of the proposed method is validated on the publicly available SCZ EEG dataset. The contributions of the present work are as follows:

1. Designing a new class of bi-orthogonal wavelet family by utilizing generalized matrix formulation techniques with maximum vanishing moments to keep sharp roll-off. Analyzing different high and lowpass filters by varying the half-band polynomial factorization.
2. Developing a novel low-complexity bi-orthogonal wavelet filter bank for an automatic EEG-based schizophrenia detection (AESD) system.
3. Optimizing disease-specific information by selecting salient EEG channels based on Fisher score and adaptive least square SVM hyper-parameters using grey wolf algorithm. Comparing the proposed AESD system with the earlier reported methods using various performance measures.

This work is organized as follows: The methodology and dataset details are provided in Section 3. The obtained results and discussion are explored in Section 4. Finally, the present work has been concluded in Section 6.

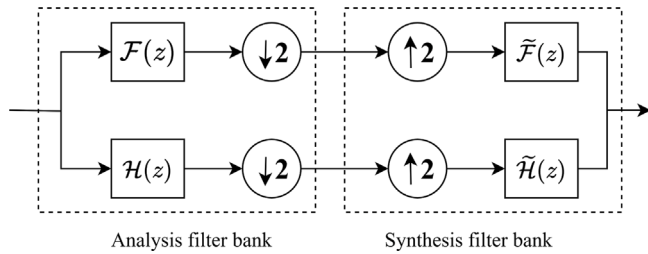


Fig. 2. General analysis-synthesis scheme using two-channel filter-bank.

2. Low-complexity bi-orthogonal wavelet filter-bank

The two-channel filter-bank (FB) is designed using finite impulse response filters, as shown in Fig. 2. Let the $F(z)$ and $H(z)$ lowpass filter (LPF) and highpass (HPF) analysis filter, respectively. To have any two-channel FB perfectly reconstructed, one has to follow conditions (2) and (3),

$$F(z)\tilde{F}(z) + H(z)\tilde{H}(z) = 2z^{-l} \quad (1)$$

where l is a delay.

$$F(z)\tilde{F}(-z) + H(z)\tilde{H}(-z) = 0 \quad (2)$$

If $F(z) = \tilde{H}(-z)$ and $\tilde{F}(z) = -\tilde{H}(-z)$, then product filter $G(z) = F(z)\tilde{F}(z)$, therefore (1) will become,

$$G(z) - G(-z) = 2z^{-l} \quad l = 1, 3, \dots \text{ odd} \quad (3)$$

The filter banks designed for perfect reconstruction have a delay of odd multiples (i.e., $l = 1, 3, 5, \dots$). This choice ensures that the signals processed through the filters remain correctly aligned after reconstruction, especially when combining the results of the lowpass and highpass filters.

The LCBWFBs can be designed using half-band polynomials $G(z)$. The steps for the design of LCBWFBs are as follows.

1. Let ρ and σ are lengths of lowpass analysis and synthesis filters, respectively. These lengths should satisfy the criteria $\text{remainder}\{(\sigma + \rho), 4\} = 0$.
2. Compute the HBP $G(z)$ of length $l = \rho + \sigma - 1$.
3. compute the unknown $u = (l - 1)/2 - 1$.
4. The maximum vanishing moments of $G(z)$ can be computed as $m = l - u - 1$. This results in $\text{remainder}\{G(z), (z + 1)^m\} = 0$.
5. Find the expression for the $Q(z) = (z + 1)^m$ and compute vector $\Phi_{1 \times u}$ containing first u coefficients of $Q(z)$ i.e. $\phi = [1, \phi_2, \phi_3, \dots, \phi_u]$.
6. Evaluate equation,

$$\mathcal{T}_{u \times u} \times \mathbb{S}_{u \times 1} = \Psi_{u \times 1} \quad (4)$$

where,

$$\mathbb{S} = [s_1, s_2, s_3, \dots, s_{u-1}, s_u]^T \text{ and } \Phi = [\xi_2, \xi_4, \xi_6, \dots, \xi_u, 0, \dots, 0]^T$$

$$\mathcal{T} = \begin{bmatrix} 1 & 0 & 0 & 0 & 0 & 0 & 0 & 0 & 0 \\ \xi_3 & \xi_2 & 1 & 0 & 0 & 0 & 0 & 0 & 0 \\ \xi_5 & \xi_4 & \xi_3 & \xi_2 & 1 & 0 & 0 & 0 & 0 \\ \cdot & \cdot \\ \xi_{u-1} & \xi_{u-2} & \cdot & \cdot & \cdot & \xi_3 & \xi_2 & 1 & 0 \\ 1 & \xi_2 & \xi_3 & \cdot & \cdot & \cdot & \cdot & \xi_{u-1} & \xi_u \\ 0 & 0 & 1 & \xi_2 & \xi_3 & \cdot & \cdot & \cdot & \xi_{u-2} \\ \cdot & \cdot \\ 0 & 0 & 0 & 0 & 0 & 0 & 0 & 1 & \xi_2 \end{bmatrix}$$

Table 2
HBP for various lengths.

m	$(\sigma + \delta)$	$D(z)$
4	8	{1, -4, 1}
6	12	{1, -6, 12.67, -6, 1}
8	16	{1, -8, 26.20, -41.6, 26.20, -8, 1}
10	20	{1, -10, 43.5, -104.3, 143.4, -104.3, 43.5, -10, 1}

7. The polynomial can be constructed as:

$$D(z) = s_{[u/2]} z^{[u/2]} + \sum_{i=0}^{[u/2]-1} s_i (z^i + z^{u-i}) \quad (5)$$

8. Evaluate the roots of $D(z)$ having phase in $[0, \pi/2]$ range and lie on the unit circle. compute the real (D_r) and imaginary (D_j) roots for various values of σ and ρ . The D_r and D_j are given by,

$$D_r = [D_{r_1}, D_{r_2}, D_{r_3}, \dots, D_{r_k}] \quad (6)$$

$$D_j = [D_{j_1}, D_{j_2}, D_{j_3}, \dots, D_{j_n}] \quad (7)$$

where k and n satisfy the relation $2k + n = u/2$.

The possible HBP with different lengths and vanishing moments are presented in Table 2.

Once the HBPs are computed, LCBWFBs with two HBPs can be designed. The creation of wavelets is that both the decomposition and reconstruction LPFs possess at least two zeros at $z = -1$. Additionally, we ensure that the filters are built using real coefficients. The steps for the construction of LCBWFB are presented in algorithms Algorithm 1.

Algorithm 1 Pseudocode for constructing LCBWFB

```

Require:  $C_b = [ ]$ , Initial = 2, final =  $ss - 1$ 
Ensure:  $ss = (1 + l)/2 - 1$ 
for Initial  $\leq$  num  $\leq$  final do
  for  $0 \leq I_1 \leq I_{im}$  do
    for  $0 \leq I_2 \leq I_{im}$  do
      for  $0 \leq J_1 \leq I_{re}$  do
        for  $0 \leq J_2 \leq I_{re}$  do
          if  $(2I_1 + 2I_2 + J_1 + J_2 == ss - num)$  then
             $C_b = [C_b; I_1 \ I_2 \ J_1 \ J_2 \ num]$ 
          end if
        end for
      end for
    end for
  end for

```

In algorithm Algorithm 1, the real and complex roots except $Z = -1$ are denoted by I_{re} and I_{im} such that magnitude of these roots less than unity. Initial and final indicates the lowest and highest number of zeros at $z = -1$ of synthesis LPF. C_b is the combination of various values of I_{re} and I_{im} . The degree of synthesis LPF is $\mathfrak{B} = 2I_{re} + 2\tilde{I}_{re} + I_{im} + \tilde{I}_{im} + 1$. The \tilde{I}_{re} and \tilde{I}_{im} are the inverse roots or real and complex roots. The residual roots of the HBP can be utilized in the design of the analysis LPF. This process is then iterated for every feasible combination present. The constructed wavelets are referred to as LCBWFB($\sigma + \rho, t$), where t is an index of combination. It forms 45 different combinations for $l = 15$. Some of the combinations are presented in Table 3. Table 4 provides the LPF coefficients for few LCBWFB($\sigma + \rho, t$) combinations. It is noted from Table 4 that all coefficients are dyadic; therefore, these are implemented on the hardware with shifts and adds.

Table 3
LCBWFB($\sigma + \rho, t$) combinations for $l = 15$.

LCBWFB	t	I_{re}	\tilde{I}_{re}	I_{im}	\tilde{I}_{im}	Z	\mathfrak{Z}	Type
(16, t)	22	1	1	0	0	4	6	B
	32	1	1	0	0	3	5	A
	36	1	0	0	0	4	5	C
	39	0	0	0	1	2	4	D
	44	0	1	0	0	2	3	C
47	0	0	0	0	2	2	B	
(20, t)	11	0	0	1	1	4	8	D
	25	0	0	0	1	4	6	D
	31	0	0	0	1	2	4	D
	32	0	0	1	0	2	4	D
	34	0	0	0	0	3	3	A
	35	0	0	0	0	2	2	B

Type A: Even-length symmetric bi-orthogonal wavelets.
Type B: Odd-length symmetric bi-orthogonal wavelets.
Type C: Even-length asymmetric bi-orthogonal wavelets.
Type D: Odd-length asymmetric bi-orthogonal wavelets.

Table 4
Different filter banks with their coefficients designed from proposed method.

LCBWFB($\sigma + \rho, t$)	Synthesis LPF coefficients
LCBWFB(16, 22)	{-264, -166, 1712, 3229, 1712, -166, -264}/4096
LCBWFB(16, 32)	{-528, 195, 3229, 3229, 196, -528}/4096
LCBWFB(20, 11)	{160, -332, -1103, 1239, 3954, 1971, -338, 17, 223}/4096
LCBWFB(20, 34)	{181, 543, 543, 181}/1024

2.1. Computational complexity and property measures

The wavelet filter properties like energy of error (E_r), time (Δt^2), frequency ($\Delta \omega^2$), and time-frequency ($\Delta t^2 \Delta \omega^2$) localization, transition-width (ΔW) of the LCBWFBs and earlier existing methods reported by Chang et al. (CLZ) [44], Tay et al. (DBT [47]), Liu and Ngan (L&N) [48], and Murugesan et al. (M&T) [49] are presented in Table 5. LCBWFBs require lower 'shifts' and 'adds' to design the same filter bank (FB) (9/7 or 11/9) as existing FBs. This reduces the computational complexity of the filters, resulting in a reduction of computational time. From the Table 5, it is clear that LCBWFBs exhibit enhanced frequency selectivity, low ΔW , optimal $\Delta t^2 \Delta \omega^2$ than earlier FBs. Notably, orthogonal wavelets maintain consistent energy distribution across average subbands. Conversely, the efficacy of bi-orthogonal wavelets depends on the length of both decomposition and reconstruction filters.

3. LCBWFBs for schizophrenia detection

3.1. EEG datasets description

In the present study, open-source EEG datasets of SCZ and NHC have been utilized. The subject details of both datasets are listed in Table 6.

The EEG dataset-A used in the present study is open-source and available at Kaggle (<https://www.kaggle.com/datasets/broach/button-tone-SCZ>). The subject details are available in Table 6. All EEG signals are recorded using 64 electrodes placed on the human scalp using a 10–20 electrode placement system. Three push-button tasks were performed on each subject. (i) Subjects have pressed a button to generate the tone immediately, (ii) Listening to the same tone passively, (iii) Pressed button without any generation of tone to observe and study the corollary discharge of SCZ patient.

The diagnosis of SCZ patients was conducted using the Structured Clinical Interview. SCZ and NHC subjects were matched for age and gender. The exclusion of SCZ, there is no other substance dependence within the past year, while NHC people were excluded if they had a history of substance dependence or a relative psychotic disorder. In the literature, wavelets have been used to remove the artifacts from the EEG signals [50]. In another study [51], A novel multi-stage EEG denoising method is reported wavelet packet decomposition (WPD)

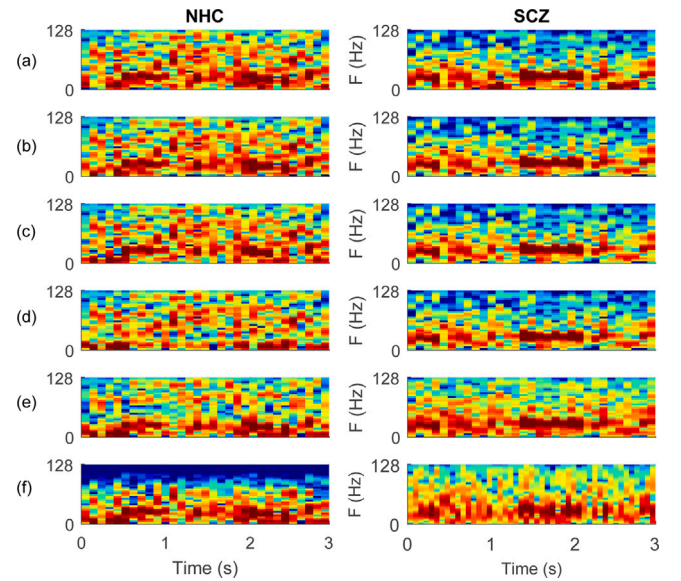


Fig. 3. An example of normal and schizophrenia EEG signals reconstructed using 5th level LCBWFB decomposition: detail coefficients at (a) first, (b) second, (c) third, (d) fourth, and (e) fifth levels and (e) approximate coefficients at fifth level.

combined with a modified non-local means (NLM) algorithm. However, pre-processing of EEG signals was carried out. The EEG signals underwent band-pass filtering between 0.5 and 100 Hz, and baseline correction was applied at -600 to -500 ms. Additionally, EEG epochs were rejected for artifacts exceeding $\pm 100 \mu V$. Further details of the dataset are provided in [52].

Fig. 3 highlights distinct neural dynamics between NHC and SCZ subjects. Each row displays the spectrogram of the AFz channels of the EEG signal reconstructed from the coefficients of a single sub-band at the 5th level of LCBWFB decomposition. The first five rows show EEG signals reconstructed from the detail coefficients from the first to fifth levels, revealing that SCZ signals exhibit increasing irregularities and erratic patterns compared to the normal signals. The last row presents the EEG signal reconstructed using the approximate coefficients at the fifth level, where normal EEG shows smoother low-frequency trends, while SCZ EEG displays disrupted, less coherent activity. Similar observations were made for several other examples from the dataset.

3.2. Channel selection

With the advancement in biomedical facilities, the acquisition of EEG data is possible with multiple channels. However, the data storage is the problem. Multichannel EEG data also increases the computational complexity and is time-consuming. To overcome this issue, significant EEG channels are selected based on Fisher's score. Fisher score finds the EEG channel subset such that the distance between two class data points should be maximized and the distance between data points of the same class minimized. The Fisher score of i th channel is computed as :

$$F_i = \frac{\sum_{m=1}^M \mathcal{P}_m (\mu_i^m - \mu_i)^2}{\sum_{m=1}^M \frac{1}{J-1} \sum_{n=1}^N (\mathcal{A}_{n,i}^m - \mu_i)^2} \quad (8)$$

where M indicates total classes; μ_i^m is the mean value of both classes; $\mathcal{A}_{n,i}^m$ is the n th observation of i th channel of m th class; \mathcal{P}_m is size of m th class; number of observations are indicated by N . The channels are selected using the Fisher score. Further, the proposed LCBWFB decomposes the selected channels' EEG signals from SCZ and NC.

Table 5
The properties comparison of proposed 9/7 and existing filter banks.

Wavelets	σ/ρ	ΔW	Adds	Shifts	E_r	Δt^2	$\Delta\omega^2$	$\Delta t^2 \Delta\omega^2$
DBT [47]	9/7	2.8472	42	58	31.83	0.4202	0.9725	0.3825
CLZ [44]	11/9	2.8365	35	156	35.74	0.4135	0.9962	0.4017
L&N [48]	9/7	2.6645	68	187	35.58	0.4162	0.9904	0.4141
M&T [49]	9/7	3.1028	74	85	33.05	0.4060	0.9720	0.3790
LCBWFB(16, 22)	9/7	1.4120	65	56	27.45	0.3975	0.9558	0.3565
LCBWFB(16, 32)	10/6	1.2480	54	50	25.96	0.4025	0.9845	0.3689
LCBWFB(20, 11)	11/9	1.2556	29	38	19.15	0.3846	0.9756	0.3648
LCBWFB(20, 34)	9/7	1.2136	34	44	23.40	0.3679	0.9749	0.3586

Table 6
Summary of EEG-based schizophrenia dataset.

Parameters	SCZ	NHC
No. of subjects	32 (26M + 6F)	49 (41M + 8F)
Age (years)	38.37 ± 13.91	40.02 ± 13.48
Female (years)	40.21 ± 12.93	38.15 ± 12.93
Male (years)	39 ± 16.98	39.33 ± 18.91
No. of channels	64	64
Duration (seconds)	3	3
Number of EEG signals	7680	7680

Table 7
Different feature sets computed to evaluate the proposed framework.

Set	Feature composition
F1	ShEn
F2	ShEn+ NoEn
F3	ShEn+NoEn+ReEn
F4	ShEn+NoEn+ReEn+ LoEn
F5	ShEn+NoEn+ReEn+ LoEn+TsEn

3.3. Features extraction

Computing the most significant features is very important in any pattern recognition system. Here, twenty-two different features were computed for each selected channel subband as presented in Table 9. The statistical method, Wilcoxon Signed-ranked (WSR) test has employed the extracted features and computed their rankings with the p - values. Out of the selected twenty-two features, only five features: Shannon entropy (ShEn), Norm entropy (NoEn), Reny's entropy (ReEn), Log energy entropy (LoEn), and Tsalli's entropy (TsEn), were chosen. The different combinations of these features are represented in Table 7 and details are available in [1,42,53].

3.4. Classification using Adaptive-LSSVM

The LSSVM has played an important role in various regression and classification applications. The LSSVM converted a non-linear problem into a linear one with its inequality constraint. The cost function to solve the linear problems is given by,

$$G(k) = \text{sign}\left\{\sum_{i=1}^I \hat{h}_r \chi_j^n B_n(k, k_j) + d_n\right\} \quad (9)$$

where I is feature vector size, real coefficients are denoted by \hat{h} , k_j is j th feature vector, The outcome of n th unit is χ_j^n , Kernel function is represented by $B_n(k, k_j)$, and d_n is bias.

The performance of the present method is compared with different kernels. The polynomial (P) kernel is given by,

$$B_n(k, k_j) = (k^T k + 1)^b \quad (10)$$

The Mexican hat (MH) kernel function is expressed as:

$$B_n(k, k_j) = \prod_{j=1}^M \left(1 - \frac{\|k - k_j\|^2}{2\tilde{\alpha}_j^2}\right) \cdot \exp\left(-\frac{\|k - k_j\|^2}{2\tilde{\alpha}_j^2}\right) \quad (11)$$

where $\tilde{\alpha}_j$ is the width controlling parameter. M is maximum number of data points. The RBF kernel function of LSSVM is represented as:

$$B_n(k, k_j) = \exp\left(\frac{-\|k - k_j\|^2}{2\tilde{\alpha}_j^2}\right) \quad (12)$$

The Morlet wavelet (MW) kernel can be defined as:

$$\prod_{j=1}^M \cos\left(\omega_0 \frac{(k - k_j)}{\tilde{\alpha}_j}\right) \cdot \exp\left(\frac{-\|k - k_j\|^2}{2\tilde{\alpha}_j^2}\right) \quad (13)$$

To find the best hyper-parameters for the objective function mentioned earlier, we utilize the GWO to obtain the optimal solution. It is inspired by the hunting method of the grey wolf. The convergence in GWO is very fast and more accurate in a very less number of iterations. The fittest solution is obtained from alpha wolves. The encirclement is defined by,

$$\bar{E} = \bar{C} \bar{Y}(k) - \bar{Y}_p(k) \quad (14)$$

$$\bar{Y}(k+1) = \bar{Y}_p(k) - \bar{A} \bar{E} \quad (15)$$

\bar{C} and \bar{A} are vectors of coefficients. The iteration number is defined by k . $\bar{Y}_p(k)$ and $\bar{Y}_p(k)$ are the wolf position and prey positions. The coefficient vectors are computed using,

$$\bar{A} = 2\bar{a} \cdot \bar{r}_1 - \bar{a}, \quad \bar{C} = 2 \cdot \bar{r}_2 \quad (16)$$

where \bar{r}_1 and \bar{r}_2 are in range of [0,1]. \bar{a} is decreasing from 2 to 0. The wolves attaching mechanism is governed by,

$$\bar{E}_\alpha = \bar{C}_1 \bar{Y}_\alpha - \bar{Y} \quad (17)$$

$$\bar{E}_\beta = \bar{C}_2 \bar{Y}_\beta - \bar{Y} \quad (18)$$

$$\bar{E}_\delta = \bar{C}_3 \bar{Y}_\delta - \bar{Y} \quad (19)$$

$$\bar{Y}_1 = \bar{Y}_\alpha - \bar{A}_1(\bar{E}_\alpha) \quad (20)$$

$$\bar{Y}_2 = \bar{Y}_\beta - \bar{A}_2(\bar{E}_\beta) \quad (21)$$

$$\bar{Y}_3 = \bar{Y}_\delta - \bar{A}_3(\bar{E}_\delta) \quad (22)$$

where, the best positions of α , β , and δ are represented by \bar{Y}_1 , \bar{Y}_2 , and \bar{Y}_3 . The hyper-parameters b , $\tilde{\alpha}$, ω_0 , and $\tilde{\sigma}$ are tuned using GWO to obtain the optimal values. In LSSVM classification, achieving optimal performance involves fine-tuning several hyper-parameters and selecting an appropriate kernel function. Lower values of these hyper-parameters tend to cause under-fitting, while higher values often result in over-fitting, leading to increased misclassification and decreased performance. To find the best settings for these hyper-parameters and kernel selection, accuracy is typically chosen as the objective function. The optimal hyper-parameters are obtained by maximizing accuracy that is represented as,

$$\text{Objective function} = \max(\text{Accuracy}) \quad (23)$$

$$\text{Accuracy (ACCY)} = \frac{T_p + T_n}{T_p + T_n + F_p + F_n}$$

where T_p , T_n , F_p , and F_n are true positive, true negative, false positive, and false negative number of samples in classification. The fittest solution is obtained from the GWO algorithm and optimized the b , $\tilde{\alpha}$, ω_0 , and $\tilde{\sigma}$ hyper-parameters.

Table 8
The Fisher score of different channels.

Rank	1	2	3	4	5	6	7	8	9	10	11	12	13	14	15	16
Ch	Afz	F2	AF4	AF7	AF4	Fp2	FPz	Cz	T7	FC4	F4	FC6	P7	F1	Fp1	FT8
Rank	17	18	19	20	21	22	23	24	25	26	27	28	29	30	31	32
Ch	F3	P9	F5	CPz	PO8	F6	FC2	F7	P5	FCz	FT7	AF3	C2	P10	P2	O1
Rank	33	34	35	36	37	38	39	40	41	42	43	44	45	46	47	48
Ch	CP5	P8	Fz	FC1	POz	Oz	Pz	PO9	P4	FC3	C1	P1	Iz	O3	TP8	C4
Rank	49	50	51	52	53	54	55	56	57	58	59	60	61	62	63	64
Ch	F8	CP6	P6	C3	CP2	C5	CP1	CP3	C6	PO4	PO7	CP4	T8	P3	PO3	TP7

Table 9
Features list with ranks and p -values using WSR test.

Feature	Rank	p -value	Rejected (\times) Selected (\checkmark)
Shannon Entropy	1	<0.05	\checkmark
Renyi entropy (ReEn)	2	<0.05	\checkmark
Norm entropy (NoEn)	3	<0.05	\checkmark
Log Energy Entropy (LoEn)	4	<0.05	\checkmark
Tsalli's entropy (TsEn)	5	<0.05	\checkmark
Higuchi's fractal dimension	6	0.0289	\times
Karl's fractal dimension	7	0.0338	\times
Band Power Delta	8	0.0429	\times
Root mean square	9	0.0462	\times
Hjorth Activity	10	0.0597	\times
Standard deviation	11	0.0659	\times
Mean	12	0.0776	\times
Simple square integral	13	0.0679	\times
Median	14	0.0883	\times
Skewness	15	0.1245	\times

3.5. Performance metrics

The performance metrics computed to validate the present method are as follows:

$$SENS = \frac{S_{ip}}{S_{ip} + S_{fn}} \quad (24)$$

$$SPEC = \frac{S_{in}}{S_{in} + S_{fp}} \quad (25)$$

$$PREC = \frac{S_{ip}}{S_{ip} + S_{fp}} \quad (26)$$

$$F1 - \text{score } (F_1) = \frac{2 \times SENS \times PREC}{SENS + PREC} \quad (27)$$

$$MCC = \frac{S_{ip} \times S_{in} - S_{fp} \times S_{fn}}{\sqrt{(S_{ip} + S_{fp})(S_{fp} + S_{fn})(S_{in} + S_{fp})(S_{in} + S_{fn})}} \quad (28)$$

where, S_{ip} is AD patient classified as AD patient, S_{fp} is the NHC subject classified as an AD patient, S_{in} is NHC subject classified as NHC subject, S_{fn} is an AD patient classified as an NHC subject. MCC is Matthews correlation coefficient.

4. Results

This method has been validated using a publicly available EEG dataset of SCZ and NHC. Initially, the EEG signals are pre-processed using EEGLAB. The artifact-free EEG signals were used to obtain the Fisher's scores for each channel. The ranks of all 64 channels according to Fisher score were presented in Table 8. From the Table 8, it is clear that the first rank is achieved by the AFz. The second rank is achieved by F2, and the lowest rank is obtained by the TP7 channel. The first five ranked EEG channels AFz, F2, AF4, AF7, and AF4 are selected for the decomposition using the proposed LCBWFBs method. Afterward, fifteen different features were computed from six different subbands (SBs) of SCZ and NHC EEG signals. The p -value of these features was obtained using WSR test. The WSR test is a non-parametric statistical test that provides the probabilistic (p) value of the given two

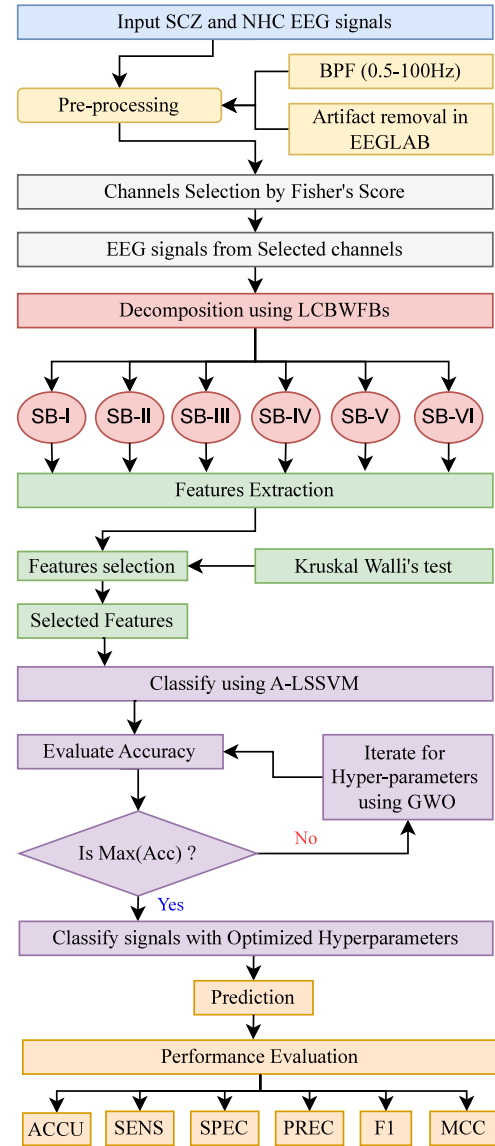


Fig. 4. Flowchart of the AESD method.

classes. The p -value of the various features are presented in Table 9. Features with a p -value less than 0.05 were selected and further used for the performance evaluation of A-LSSVM. The optimal hyperparameters of A-LSSVM were obtained from the GWO by an iterative process. The detailed flow of the AESD method is presented in Fig. 4. The performance of proposed L1-LCBWFB(16, 22), L2-LCBWFB(16, 32), L3-LCBWFB(20, 11), L4-LCBWFB(20, 34), and L5-LCBWFB(16, 47) for the different kernel functions (P, MH, MW, and RBF) of LS-SVM model are presented in the Fig. 5(a). From Fig. 5(a), it is proved that the RBF kernel obtained maximum accuracy of 94.85% using L4-based

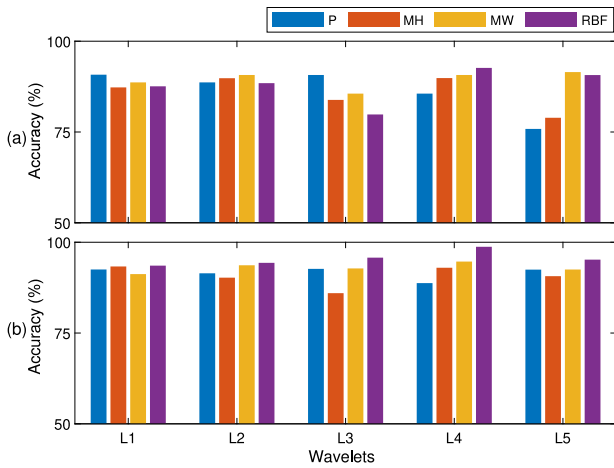


Fig. 5. Performance of the proposed LCBWFBs-based features with 10-fold CV using the (a) LSSVM and (b) A-LSSVM, where L1-LCBWFB(16, 22), L2-LCBWFB(16, 32), L3-LCBWFB(20, 11), L4-LCBWFB(20, 34), and L5-LCBWFB(16, 47).

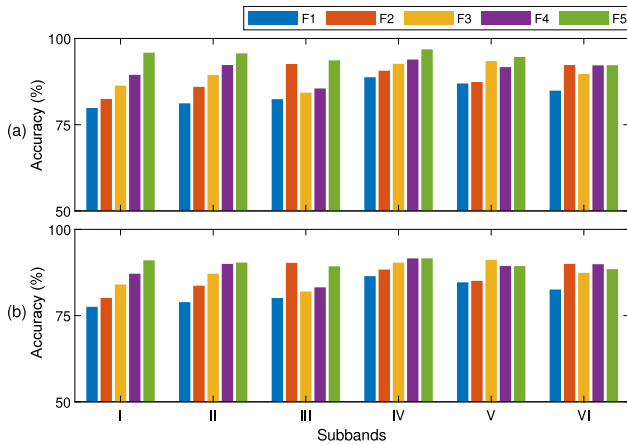


Fig. 6. Performance of different feature sets for (a) 10-fold CV and (b) LOSO CV.

Table 10 Performance (in %) of six subbands using LCBWFB(20,34) 9/7 for one channel EEG signal features.

CV	SBs	ACCY	SENS	SPEC	PREC	F ₁	MCC
10-fold	I	95.88	94.3	97.5	96.57	92.31	98.65
	II	95.68	93.25	96.34	95.66	90.39	98.02
	III	93.67	93.67	92.15	95.57	90.31	95.65
	IV	96.84	95.95	96.97	94.56	92.37	96.97
	V	94.66	92.31	94.50	91.72	88.28	95.44
	VI	92.25	91.15	93.64	92.30	93.95	89.39
LOSO	I	93.33	92.3	93.77	90.79	90.69	92.17
	II	92.68	91.52	90.64	92.98	88.76	93.43
	III	91.59	90.60	89.5	91.46	89.72	92.67
	IV	93.92	92.56	90.45	90.94	89.98	96.97
	V	91.66	90.78	92.89	91.72	88.28	95.44
	VI	90.78	88.52	90.85	91.63	89.89	89.39

features among other kernels (MH, MW, and P) and filter banks (L1, L2, L3, and L5). The performance of proposed wavelets with A-LSSVM is presented in Fig. 5(b). It is clear that the proposed AESD system achieved the maximum accuracy of 97.60% from L4-based features and A-LSSVM with RBF kernel. This performance is obtained using F5 features from all SBs. The purpose of the present work is to reduce the computational complexity by reducing the number of SB features. Therefore, the performance metrics of each SB for 10-fold CV and LOSO CV are shown in Table 10. The 10-fold cross-validation is a popular

Table 11 Classification accuracy of different feature sets for different subbands.

CV	Subband	F1	F2	F3	F4	F5
10-fold	I	79.85	82.45	86.33	89.45	95.88
	II	81.20	85.98	89.46	92.30	95.68
	III	82.40	92.60	84.30	85.50	93.67
	IV	88.75	90.66	92.66	93.89	96.84
	V	86.95	87.38	93.44	91.70	94.66
	VI	84.87	92.30	89.70	92.20	92.25
LOSO	I	77.55	80.15	84.03	87.15	93.33
	II	78.90	83.68	87.16	90.00	92.68
	III	80.10	90.30	82.00	83.20	91.59
	IV	86.45	88.36	90.36	91.59	93.92
	V	84.65	85.08	91.14	89.40	91.66
	VI	82.57	90.00	87.4	89.90	90.78

technique used to assess model performance by splitting the dataset into 10 equal-sized subsets or “folds”. In each of the 10 iterations, one fold is used as the test set, while the remaining 9 folds are used to train the model. This process is repeated 10 times, with each fold serving as the test set once, ensuring that every data point is used for both training and testing. This performance is obtained by the F5 feature set. The best accuracy of 96.84% is achieved from the IVth subband using 10-fold CV and A-LSSVM. Whereas LOSO CV obtained the best accuracy of 93.92% for the same subband. The lowest SCZ detection rate is reported by features from VIth subband. While the model performs well in terms of both accuracy and specificity, a sensitivity of 95.95% suggests that there may still be some room for improvement, particularly in correctly identifying positive instances (true positives) in the data. From Table 10, it is noted that the performance of the 10-fold CV is better than the LOSO CV. LOSO performs poorly when the datasets do not contain large data sizes.

5. Discussion

5.1. Effect of feature sets

The performance of the proposed AESD system is computed for each feature set (F1, F2, F3, F4, and F5) and each subband. This performance is presented in Table 11. The barplot of accuracies is shown in Fig. 6. The F5 feature set is a combination of all five features. Hence, the best performance has been achieved from the fourth subband-based F5 feature set with a 10-fold CV. However, the lowest SCZ detection rate was obtained from the first subband-based F1 features. The accuracy of all the features has been reduced in LOSO CV, independent of the subband. Fig. 6 clearly indicates that the F5 feature set from the fourth subband is the most effective solution for distinguishing SCZ from NHC. Although increasing the number of features improves accuracy, it also raises computational complexity, creating a trade-off between these two factors. The proposed AESD system achieves the highest classification accuracy while maintaining lower computational complexity.

5.2. Performance comparison

The comparative analysis of the proposed method with the current SOTA techniques is presented in Table 12. Zang et al. [54] employed age, ERP, educational, and conditional factors to distinguish between individuals with NHC and SCZ. Utilizing these variables, they achieved an 81.10% classification accuracy using an RF model. Their findings suggest that increasing the number of features leads to improved accuracy in classification. The study in [55] computed the EMD-based five features selected using the WSR test. This model achieved 89.59% accuracy from the second IMF and ensemble bagged tree. Khare et al. presented EWT-based features with various machine-learning models to

Table 12
Related state-of-art methods for diagnosis of Schizophrenia.

Ref.	Method	Classifier	ACCU	SENS	SPEC
[54]	Statistical features	RF	80.15	–	–
[1]	EWT	SVM	89.59	89.76	89.32
[55]	EMD	EBT	89.94	89.36	89.64
[23]	FTQWT	F-LSSVM	91.39	92.65	93.22
[24]	OVM	OELM	92.93	97.15	91.06
[17]	Correlation feature	AdaBoost	92.85	93.30	92.30
[56]	Electrical marker	DNN	92.00	–	–
[33]	PSD and HP	CNN	94.04	92.70	95.31
[57]	VAM connectivity	GTCN	95.00	–	–
[58]	TQWT	KNN	95.24	97.01	94.06
This work	LCBWFB	A-LSSVM	96.84	95.95	96.97

detect SCZ. Their study obtained an accuracy of 88.70% with SVM and five features of a single subband. Gao et al. [59] investigated the higher dimensional electrical features such as connectivity, spectral, evoked, and information theory. The DNN has been used to classify these features and obtained 92% classification rate. In another study [60], explored the TQWT-based 25 statistical features has achieved 95.84% accuracy with KNN. In studies reported in [1,23,55,58] utilized all channel EEG signals and different decomposition methods with maximum accuracy of 95%. The newly designed LCBWFB with ALSSVM achieved maximum accuracy of 96.84% using five-channel EEG signals. From Table 12, it is clear that the performance of the presently developed method is superior to the SOTA methods. The present method is automatic and does not require any predefined parameters for the classification.

5.3. Clinical significance

- Real-time, non-invasive detection: Emphasized how the methods could be used for real-time diagnosis in clinical settings, making it a practical alternative to traditional, more expensive methods.
- Improved diagnostic accuracy: Highlighted the high sensitivity and specificity, which are crucial for ensuring accurate diagnosis and minimizing errors in clinical practice.
- Feasibility for routine screening: Focused on the practical aspect of using this approach for routine clinical applications, given the small set of features required for the model.
- Impact on early intervention: Stressed the potential of the method to enable early detection, which is critical for improving patient outcomes in schizophrenia.

5.4. Limitations and future work

The newly introduced LCBWFBs demonstrate superior performance compared to existing models, despite they exhibit certain limitations. This method has been tested on a publicly available EEG dataset for SCZ; however, the population size of the dataset is relatively small. Various factors, including age, gender, and medication use, can significantly influence a model's performance. Specifically, the proposed model shows promising results in analyzing EEG signals from younger SCZ patients. Based on the findings of this research, several future explorations can be considered:

- Expanding the EEG SCZ dataset and including various demographics, disease stages, fuzzy concepts, and explainable AI techniques can improve the generalizability of this work.
- Implementing a real-time system could facilitate disease monitoring and prompt intervention, thereby enhancing healthcare outcomes.
- Lastly, comprehensive clinical validations are necessary to evaluate the model's performance extensively across various scenarios, ensuring its practicality and safety for integration into healthcare practices.

6. Conclusion

This paper proposes a novel class of less complex bi-orthogonal wavelet filter banks (LCBWFB) for detecting SCZ. The analysis and synthesis filters of LCBWFB are designed using a generalized matrix formulation method with maximum vanishing moments to keep sharp roll-off. The different combinations of these wavelets are possible by changing the parameters. The proposed wavelets are effective and less complex compared to other wavelets. Therefore, the most suitable wavelets for SCZ detection are obtained. Initially, the most discriminate channels were selected using the Fisher score. The EEG signals from selected channels were decomposed into six subbands using proposed analysis wavelet filters. The obtained subbands were utilized to extract various features. Of these features, only five were selected using the WSR test. These features are utilized to train and test adaptive least square support vector machines (A-LSSVM). The kernel and hyperparameters of A-LSSVM are determined using the GWO to ensure that the accuracy of each subband can be optimized. The efficacy of this study is evaluated using a publicly accessible dataset, which shows a classification accuracy of 96.84% using only characteristics of five subbands through a 10-fold CV. Significantly, our method outperforms existing techniques in detecting SCZ, achieving 2% higher accuracy with a smaller number of features.

Expanding the EEG SCZ dataset to include diverse demographics along with incorporating explainable AI techniques with new deep learning models, can enhance the generalizability of this work. Additionally, thorough clinical validations are essential to rigorously assess the model's performance across various scenarios, ensuring its reliability, practicality, and safety for seamless integration into healthcare practices.

CRedit authorship contribution statement

Digambar V. Puri: Writing – original draft, Visualization, Validation, Software, Resources, Methodology, Conceptualization. **Pramod H. Kachare:** Writing – original draft, Visualization, Validation, Software, Resources, Methodology, Conceptualization. **Ibrahim Al-Shourbaji:** Writing – review & editing, Writing – original draft, Visualization, Supervision, Software, Resources, Methodology, Conceptualization. **Abdoh Jabbari:** Writing – review & editing, Methodology, Conceptualization. **Raimund Kirner:** Writing – review & editing, Methodology, Conceptualization. **Abdalla Alameen:** Writing – review & editing, Conceptualization.

Funding

The article processing charge for this paper was funded by the University of Hertfordshire, United Kingdom.

Declaration of competing interest

The authors declare that they have no known competing financial interests or personal relationships that could have appeared to influence the work reported in this paper.

Acknowledgments

The authors would like to thank the University of Hertfordshire, United Kingdom for providing the research funding for this article.

Data availability

The EEG datasets used in this work are publicly available.

References

- [1] Smith K. Khare, Varun Bajaj, A self-learned decomposition and classification model for schizophrenia diagnosis, *Comput. Methods Programs Biomed.* (ISSN: 0169-2607) 211 (2021) 106450, <http://dx.doi.org/10.1016/j.cmpb.2021.106450>.
- [2] Annemarie Wolff, Georg Northoff, Temporal imprecision of phase coherence in schizophrenia and psychosis—dynamic mechanisms and diagnostic marker, *Mol. Psychiatry* 29 (2) (2024) 425–438.
- [3] Kyung-Ok Cho, Hyun-Jong Jang, Comparison of different input modalities and network structures for deep learning-based seizure detection, *Sci. Rep.* 10 (1) (2020) 122.
- [4] Hui Yang, Ling He, Wen Li, Qi Zheng, Yuanyuan Li, Xiujuan Zheng, Jing Zhang, An automatic detection method for schizophrenia based on abnormal eye movements in reading tasks, *Expert Syst. Appl.* (ISSN: 0957-4174) 238 (2024) 121850, <http://dx.doi.org/10.1016/j.eswa.2023.121850>.
- [5] Afshin Shoeibi, Navid Ghassemi, Marjane Khodatars, Parisa Moridian, Abbas Khosravi, Assef Zare, Juan M. Gorriz, Amir Hossein Chale-Chale, Ali Khadem, U. Rajendra Acharya, Automatic diagnosis of schizophrenia and attention deficit hyperactivity disorder in rs-fMRI modality using convolutional autoencoder model and interval type-2 fuzzy regression, *Cogn. Neurodynamics* 17 (6) (2023) 1501–1523, <http://dx.doi.org/10.1007/s11571-022-09897-w>.
- [6] Anis Malekzadeh, Assef Zare, Mahdi Yaghoobi, Roohallah Alizadehsani, Automatic diagnosis of epileptic seizures in eeg signals using fractal dimension features and convolutional autoencoder method, *Big Data Cogn. Comput.* (ISSN: 2504-2289) 5 (4) (2021) <http://dx.doi.org/10.3390/bdcc5040078>.
- [7] Sandeep B. Sangle, Pramod H. Kachare, Digambar V. Puri, Ibrahim Al-Shoubarji, Abdoh Jabbari, Raimund Kirner, Explaining electroencephalogram channel and subband sensitivity for alcoholism detection, *Comput. Biol. Med.* (ISSN: 0010-4825) 188 (2025) 109826, <http://dx.doi.org/10.1016/j.compbiomed.2025.109826>.
- [8] Samannaya Adhikari, Nitin Choudhury, Swastika Bhattacharya, Nabamita Deb, Daisy Das, Rajdeep Ghosh, Souvik Phadikar, Ebrahim Ghaderpour, Analysis of frequency domain features for the classification of evoked emotions using EEG signals, *Exp. Brain Res.* 243 (3) (2025) 65.
- [9] Digambar V. Puri, Jayanand P. Gawande, Pramod H. Kachare, Ibrahim Al-Shoubarji, Optimal time-frequency localized wavelet filters for identification of Alzheimer's disease from eeg signals, *Cogn. Neurodynamics* 19 (1) (2025) 12.
- [10] Digambar V. Puri, Sanjay L. Nalbalwar, Anil B. Nandgaonkar, Jayanand P. Gawande, Abhay Wagh, Automatic detection of Alzheimer's disease from EEG signals using low-complexity orthogonal wavelet filter banks, *Biomed. Signal Process. Control.* (ISSN: 1746-8094) 81 (2023) 104439, <http://dx.doi.org/10.1016/j.bspc.2022.104439>.
- [11] Shalbhya Ali, Suraiya Parveen, Ihtiram Raza Khan, Bhavya Alankar, Schizophrenia detection using distributed activation function-based statistical attentional bidirectional-long short-term memory, *Comput. Biol. Med.* (ISSN: 0010-4825) 186 (2025) 109650, <http://dx.doi.org/10.1016/j.compbiomed.2024.109650>.
- [12] S. Senthil Kumar, A.R. Venmathi, Yuvaraja Thangavel, L. Raja, ResDense Fusion: enhancing schizophrenia disorder detection in EEG data through ensemble fusion of deep learning models, *Neural Comput. Appl.* 37 (4) (2025) 2411–2433.
- [13] Guimei Yin, Jie Yuan, Yanjun Chen, Guangxing Guo, Dongli Shi, Lin Wang, Zilong Zhao, Yanli Zhao, Manjie Zhang, Yuan Dong, et al., Schizophrenia recognition based on three-dimensional adaptive graph convolutional neural network, *Sci. Rep.* 15 (1) (2025) 4067.
- [14] Mingkan Shen, Peng Wen, Bo Song, Yan Li, 3D convolutional neural network for schizophrenia detection using as EEG-based functional brain network, *Biomed. Signal Process. Control.* (ISSN: 1746-8094) 89 (2024) 105815, <http://dx.doi.org/10.1016/j.bspc.2023.105815>.
- [15] Muhammad Hussain, Noudha Abdulrahman Alsalooli, Norah Almaghrabi, Emad-ul-Haq Qazi, Schizophrenia detection on eeg signals using an ensemble of a lightweight convolutional neural network, *Appl. Sci.* (ISSN: 2076-3417) 14 (12) (2024) <http://dx.doi.org/10.3390/app14125048>, URL <https://www.mdpi.com/2076-3417/14/12/5048>.
- [16] Sumair Aziz, Muhammad Umar Khan, Khushbakht Iqtidar, Raul Fernandez-Rojas, Diagnosis of schizophrenia using eeg sensor data: A novel approach with automated log energy-based empirical wavelet reconstruction and cepstral features, *Sensors* (ISSN: 1424-8220) 24 (20) (2024) <http://dx.doi.org/10.3390/s24206508>, URL <https://www.mdpi.com/1424-8220/24/20/6508>.
- [17] T. Sunil Kumar, Kandala N.V.P.S. Rajesh, Shishir Maheswari, Vivek Kanhangad, U. Rajendra Acharya, Automated schizophrenia detection using local descriptors with EEG signals, *Eng. Appl. Artif. Intell.* (ISSN: 0952-1976) 117 (2023) 105602, <http://dx.doi.org/10.1016/j.engappai.2022.105602>.
- [18] Pankaj Kumar Sahu, Artificial intelligence system for verification of schizophrenia via theta-eeg rhythm, *Biomed. Signal Process. Control.* (ISSN: 1746-8094) 81 (2023) 104485, <http://dx.doi.org/10.1016/j.bspc.2022.104485>.
- [19] J. Ruiz de Miras, A.J. Ibáñez Molina, M.F. Soriano, S. Iglesias-Parro, Schizophrenia classification using machine learning on resting state EEG signal, *Biomed. Signal Process. Control.* (ISSN: 1746-8094) 79 (2023) 104233, <http://dx.doi.org/10.1016/j.bspc.2022.104233>.
- [20] Anil Aksöz, Doğukan Akyüz, Furkan Bayir, Nevzat Can Yıldız, Firat Orhanbulucu, Fatma Latifoğlu, Analysis and classification of schizophrenia using event related potential signals, *Comput. Sci.* (2022) 32–36.
- [21] Ahmadreza Keihani, Seyed Saman Sajadi, Mahsa Hasani, Fabio Ferrarelli, Bayesian optimization of machine learning classification of resting-state eeg microstates in schizophrenia: A proof-of-concept preliminary study based on secondary analysis, *Brain Sci.* (ISSN: 2076-3425) 12 (11) (2022) <http://dx.doi.org/10.3390/brainsci12111497>.
- [22] Ahmad Zandbagleh, Sattar Mirzakuchaki, Mohammad Reza Daliri, Preethi Premkumar, Saeid Sanei, Classification of low and high schizotypy levels via evaluation of brain connectivity, *Int. J. Neural Syst.* 32 (04) (2022) 2250013, <http://dx.doi.org/10.1142/S0129065722500137>, PMID: 35236254.
- [23] Smith K. Khare, Varun Bajaj, A hybrid decision support system for automatic detection of schizophrenia using eeg signals, *Comput. Biol. Med.* (ISSN: 0010-4825) 141 (2022) 105028, <http://dx.doi.org/10.1016/j.compbiomed.2021.105028>.
- [24] Smith K. Khare, Nikhil B. Gaikwad, Varun Bajaj, VHRS: A Novel Variational Mode Decomposition and Hilbert Transform-Based EEG Rhythm Separation for Automatic ADHD Detection, *IEEE Trans. Instrum. Meas.* 71 (2022) 1–10, <http://dx.doi.org/10.1109/TIM.2022.3204076>.
- [25] Kandala N.V.P.S. Rajesh, T. Sunil Kumar, Schizophrenia detection in adolescents from eeg signals using symmetrically weighted local binary patterns, in: 43rd Annual International Conference of the IEEE Engineering in Medicine and Biology Society, EMBC, 2021, pp. 963–966, <http://dx.doi.org/10.1109/EMBC46164.2021.9630232>.
- [26] Smith K. Khare, Varun Bajaj, Time–frequency representation and convolutional neural network-based emotion recognition, *IEEE Trans. Neural Netw. Learn. Syst.* 32 (7) (2021) 2901–2909, <http://dx.doi.org/10.1109/TNNLS.2020.3008938>.
- [27] Sunil Kumar Prabhakar, Harikumar Rajaguru, Seong-Whan Lee, A framework for schizophrenia eeg signal classification with nature inspired optimization algorithms, *IEEE Access* 8 (2020) 39875–39897, <http://dx.doi.org/10.1109/ACCESS.2020.2975848>.
- [28] Chun-Ren Phang, Fuad Noman, Hadri Hussain, Chee-Ming Ting, Hernando Ombao, A multi-domain connectome convolutional neural network for identifying schizophrenia from EEG connectivity patterns, *IEEE J. Biomed. Heal. Inform.* 24 (5) (2020) 1333–1343, <http://dx.doi.org/10.1109/JBHI.2019.2941222>.
- [29] Carlos Alberto Torres Naira, Cristian Jos, et al., Classification of people who suffer schizophrenia and healthy people by EEG signals using deep learning, *Int. J. Adv. Comput. Sci. Appl.* 10 (10) (2019) <http://dx.doi.org/10.14569/IJACSA.2019.0101067>.
- [30] V. Jahnumah, Shu Lih Oh, V. Rajinikanth, Edward J. Ciaccio, Kang Hao Cheong, N. Arunkumar, U. Rajendra Acharya, Automated detection of schizophrenia using nonlinear signal processing methods, *Artif. Intell. Med.* (ISSN: 0933-3657) 100 (2019) 101698, <http://dx.doi.org/10.1016/j.artmed.2019.07.006>, URL <https://www.sciencedirect.com/science/article/pii/S0933365719303628>.
- [31] A. Nikhil Chandran, Karthik Sreekumar, D.P. Subha, EEG-based automated detection of schizophrenia using long short-term memory (LSTM) network, in: *Advances in Machine Learning and Computational Intelligence: Proceedings of ICMLCI 2019*, Springer, 2021, pp. 229–236.
- [32] Zülfiyar Aslan, Mehmet Akin, Automatic detection of schizophrenia by applying deep learning over spectrogram images of eeg signals, *Trait. Signal* 37 (2) (2020).
- [33] Kuldeep Singh, Sukhjeet Singh, Jyoteesh Malhotra, Spectral features based convolutional neural network for accurate and prompt identification of schizophrenic patients, *Proc. Inst. Mech. Eng. Part H: J. Eng. Med.* 235 (2) (2021) 167–184, <http://dx.doi.org/10.1177/0954411920966937>, PMID: 33124526.
- [34] Buettner2020HICSS, Development of a machine learning based algorithm to accurately detect schizophrenia based on one-minute EEG recordings, 2020.
- [35] Jeong-Youn Kim, Hyun Seo Lee, Seung-Hwan Lee, EEG Source Network for the Diagnosis of Schizophrenia and the Identification of Subtypes Based on Symptom Severity—A Machine Learning approach, *J. Clin. Med.* (ISSN: 2077-0383) 9 (12) (2020) <http://dx.doi.org/10.3390/jcm9123934>.
- [36] Ahmad Shalhaf, Sara Bagherzadeh, Arash Maghsoudi, Transfer learning with deep convolutional neural network for automated detection of schizophrenia from eeg signals, *Phys. Eng. Sci. Med.* 43 (2020) 1229–1239.
- [37] Palani Thanaraj Krishnan, Alex Noel Joseph Raj, Parvathavarthini Balasubramanian, Yuanzhu Chen, Schizophrenia detection using multivariate empirical mode decomposition and entropy measures from multichannel EEG signal, *BioCybern. Biomed. Eng.* (ISSN: 0208-5216) 40 (3) (2020) 1124–1139, <http://dx.doi.org/10.1016/j.bbe.2020.05.008>.
- [38] Manish Sharma, U. Rajendra Acharya, Automated detection of schizophrenia using optimal wavelet-based l1 norm features extracted from single-channel EEG, *Cogn. Neurodynamics* 15 (4) (2021) 661–674.
- [39] Kritiprasanna Das, Ram Bilas Pachori, Schizophrenia detection technique using multivariate iterative filtering and multichannel EEG signals, *Biomed. Signal Process. Control.* (ISSN: 1746-8094) 67 (2021) 102525, <http://dx.doi.org/10.1016/j.bspc.2021.102525>.
- [40] Bethany Gosala, Pappu Dindayal Kapgate, Priyanka Jain, Rameshwar Nath Chaurasia, Manjari Gupta, Wavelet transforms for feature engineering in EEG data processing: An application on schizophrenia, *Biomed. Signal Process. Control.* (ISSN: 1746-8094) 85 (2023) 104811, <http://dx.doi.org/10.1016/j.bspc.2023.104811>.
- [41] Ingrid Daubechies, The wavelet transform, time-frequency localization and signal analysis, *IEEE Trans. Inform. Theory* 36 (5) (1990) 961–1005.

- [42] Digambar V. Puri, Jayanand P. Gawande, Jaswantsing L. Rajput, Sanjay L. Nalbalwar, A novel optimal wavelet filter banks for automated diagnosis of Alzheimer's disease and mild cognitive impairment using electroencephalogram signals, *Decis. Anal. J.* (ISSN: 2772-6622) 9 (2023) 100336, <http://dx.doi.org/10.1016/j.dajour.2023.100336>.
- [43] Stéphane Mallat, *A Wavelet Tour of Signal Processing*, Elsevier, 1999.
- [44] L. Cheng, D.L. Liang, Z.H. Zhang, Popular biorthogonal wavelet filters via a lifting scheme and its application in image compression, *Vis. Image Signal Process. IEE Proc.* 150 (2003) 227–232, <http://dx.doi.org/10.1049/ip-vis:20030557>.
- [45] Bhushan D. Patil, Pushkar G. Patwardhan, Vikram M. Gadre, On the design of fir wavelet filter banks using factorization of a halfband polynomial, *IEEE Signal Process. Lett.* 15 (2008) 485–488.
- [46] Hossein Rezaei, Omid Bozorg-Haddad, Xuefeng Chu, Grey wolf optimization (gwo) algorithm, *Adv. Optim. Nature-Inspired Algorithms* (2018) 81–91.
- [47] D.B.H. Tay, Rationalizing the coefficients of popular biorthogonal wavelet filters, *IEEE Trans. Circuits Syst. Video Technol.* 10 (6) (2000) 998–1005, <http://dx.doi.org/10.1109/76.867939>.
- [48] Yu Liu, King Ngi Ngan, Weighted adaptive lifting-based wavelet transform for image coding, *IEEE Trans. Image Process.* 17 (4) (2008) 500–511, <http://dx.doi.org/10.1109/TIP.2008.917104>.
- [49] Selvaraju Murugesan, David B.H. Tay, New techniques for rationalizing orthogonal and biorthogonal wavelet filter coefficients, *IEEE Trans. Circuits Syst. I. Regul. Pap.* 59 (3) (2012) 628–637, <http://dx.doi.org/10.1109/TCSI.2011.2165415>.
- [50] Matteo Dora, David Holcman, Adaptive single-channel eeg artifact removal with applications to clinical monitoring, *IEEE Trans. Neural Syst. Rehabil. Eng.* 30 (2022) 286–295, <http://dx.doi.org/10.1109/TNSRE.2022.3147072>.
- [51] Souvik Phadikar, Nidul Sinha, Rajdeep Ghosh, Ebrahim Ghaderpour, Automatic muscle artifacts identification and removal from single-channel eeg using wavelet transform with meta-heuristically optimized non-local means filter, *Sensors* (ISSN: 1424-8220) 22 (8) (2022) <http://dx.doi.org/10.3390/s22082948>, URL <https://www.mdpi.com/1424-8220/22/8/2948>.
- [52] Judith M. Ford, Vanessa A. Palzes, Brian J. Roach, Daniel H. Mathalon, Did I do that? Abnormal predictive processes in schizophrenia when button pressing to deliver a tone, *Schizophr. Bull.* (ISSN: 0586-7614) 40 (4) (2013) 804–812, <http://dx.doi.org/10.1093/schbul/sbt072>.
- [53] Majid Aljalal, Marta Molinas, Saeed A. Aldosari, Khalil AlSharabi, Akram M. Abdurraqeab, Fahd A. Alturki, Mild cognitive impairment detection with optimally selected EEG channels based on variational mode decomposition and supervised machine learning, *Biomed. Signal Process. Control.* (ISSN: 1746-8094) 87 (2024) 105462, <http://dx.doi.org/10.1016/j.bspc.2023.105462>.
- [54] Lei Zhang, EEG signals classification using machine learning for the identification and diagnosis of schizophrenia, in: 2019 41st Annual International Conference of the Ieee Engineering in Medicine and Biology Society, EMBC, IEEE, 2019, pp. 4521–4524.
- [55] Siuly Siuly, Smith K. Khare, Varun Bajaj, Hua Wang, Yanchun Zhang, A computerized method for automatic detection of schizophrenia using EEG signals, *IEEE Trans. Neural Syst. Rehabil. Eng.* 28 (11) (2020) 2390–2400.
- [56] Zhifen Guo, Lezhou Wu, Yun Li, Beilin Li, Deep neural network classification of eeg data in schizophrenia, in: 2021 IEEE 10th Data Driven Control and Learning Systems Conference, DDCLS, 2021, pp. 1322–1327, <http://dx.doi.org/10.1109/DDCLS52934.2021.9455509>.
- [57] Chun-Ren Phang, Chee-Ming Ting, S. Balqis Samdin, Hernando Ombao, Classification of eeg-based effective brain connectivity in schizophrenia using deep neural networks, in: Michel Maharbiz, Cynthia Chestek (Eds.), 9th International IEEE EMBS Conference on Neural Engineering, in: International IEEE/EMBS Conference on Neural Engineering, NER, United States of America, ISBN: 9781538679227, 2019, pp. 401–406, <http://dx.doi.org/10.1109/NER.2019.8717087>.
- [58] Mehmet Baygin, An accurate automated schizophrenia detection using TQWT and statistical moment based feature extraction, *Biomed. Signal Process. Control.* (ISSN: 1746-8094) 68 (2021) 102777, <http://dx.doi.org/10.1016/j.bspc.2021.102777>.
- [59] Zhifen Guo, Jiao Wang, Tianyu Jing, Longyue Fu, Investigating the interpretability of schizophrenia EEG mechanism through a 3DCNN-based hidden layer features aggregation framework, *Comput. Methods Programs Biomed.* (ISSN: 0169-2607) 247 (2024) 108105, <http://dx.doi.org/10.1016/j.cmpb.2024.108105>.
- [60] Mehmet Baygin, Prabal Datta Barua, Subrata Chakraborty, Ilknur Tuncer, Sengul Dogan, Elizabeth Palmer, Turker Tuncer, Aditya P. Kamath, Edward J. Ciaccio, U. Rajendra Acharya, Ccpnet136: automated detection of schizophrenia using carbon chain pattern and iterative tqwt technique with eeg signals, *Physiol. Meas.* 44 (3) (2023) 035008, <http://dx.doi.org/10.1088/1361-6579/acb03c>.